Eupatilin improves cilia defects in human CEP290 ciliopathy models

Corral-Serrano JC[1*§], Sladen PE[1*], Ottaviani D[1,2*], Rezek FO[1], Jovanovic K[1], Athanasiou D[1], van der Spuy, J[1], Mansfield, BC[3] and Cheetham ME[1§]

[1]UCL Institute of Ophthalmology, 11-43 Bath Street, London, EC1V 9EL UK;

[2]Department of Biology, University of Padova, Padova, Italy.

[3]Eunice Kennedy Shriver National Institute of Child Health and Human Development, National Institutes of Health, Bethesda, MD USA.

*equal contribution

§ correspondence to Dr Julio Corral Serrano j.serrano@ucl.ac.uk ; Professor Mike Cheetham michael.cheetham@ucl.ac.uk

Abstract

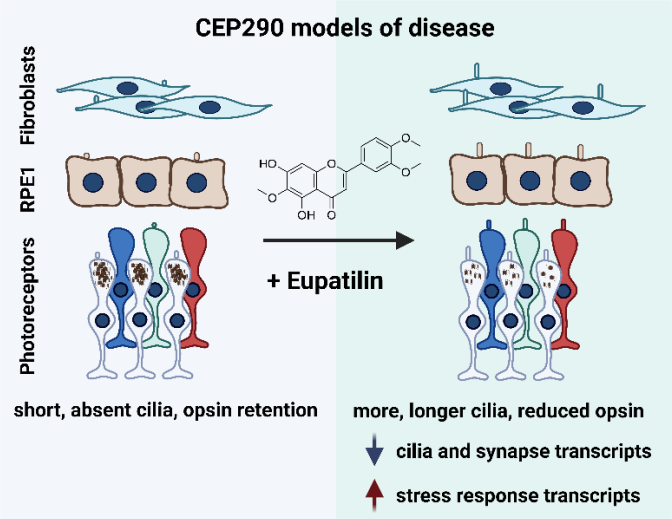

The photoreceptor outer segment is a highly specialized primary cilium essential for phototransduction and vision. Biallelic pathogenic variants in the cilia-associated gene *CEP290* cause non-syndromic Leber congenital amaurosis 10 (LCA10) and syndromic diseases, where the retina is also affected. While RNA antisense oligonucleotides and gene editing are potential treatment options for the common deep intronic variant c.2991+1655A>G in *CEP290*, there is a need for variant-independent approaches that could be applied to a broader spectrum of ciliopathies. Here, we generated several distinct human models of *CEP290*-related retinal disease and investigated the effects of the flavonoid eupatilin as a potential treatment. Eupatilin improved cilium formation and length in CEP290 LCA10 patient-derived fibroblasts, in gene-edited *CEP290* knockout (CEP290 KO) RPE1 cells, and in both CEP290 LCA10 and CEP290 KO iPSCs-derived retinal organoids. Furthermore, eupatilin reduced rhodopsin retention in the outer nuclear layer of CEP290 LCA10 retinal organoids. Eupatilin altered gene transcription in retinal organoids, by modulating the expression of rhodopsin, and by targeting cilia and synaptic plasticity pathways. This work sheds light into the mechanism of action of eupatilin, and supports its potential as a variant-independent approach for *CEP290*-associated ciliopathies.

Introduction

Primary cilia are microtubule-based organelles that function as a sensor of the extracellular environment. Photoreceptor cells contain a highly specialized primary cilium called the outer segment that is essential for detecting light and initiating phototransduction. Diseases that affect the function of cilia genes are termed ciliopathies, with many having retinal degeneration as a common feature. Biallelic variants in the cilia gene *CEP290 (NPHP6)* can cause a series of syndromic ciliopathies including Joubert Syndrome, nephronophthisis, Meckel-Gruber syndrome and Senior-Loken syndrome (1–3). *CEP290* is also the most affected gene in non-syndromic Leber Congenital Amaurosis (type 10, LCA10), characterized by early vision loss due to photoreceptor cell death (4,5). The most common *CEP290* deep intronic variant, c.2991+1655A>G, results in aberrant splicing and the inclusion of a cryptic exon containing an immediate premature stop codon, p.C998X (4). Current therapeutic options to treat LCA10 are limited and have focused on this deep intronic variant (6). For example, a gene-editing approach directed to this intronic variant is currently in clinical trials (7). Moreover, treatment of the *CEP290* c.2991+1655A>G variant with the RNA antisense oligonucleotide (AON) sepofarsen (QR-110) restored CEP290 function in preclinical models (8), improved visual acuity in phase Ib/II clinical trials (9–11) and cone sensitivity in individuals with congenital blindness (12). The effects were long lasting, with improvements reported over 12 months following a single injection (10). However, in a placebo-controlled phase II/III clinical trial, sepofarsen did not meet the primary endpoint of best corrected visual acuity at month 12, resulting in the discontinuation of the clinical trials (13). Considering that other *CEP290* pathogenic variants contributing to LCA10 or other syndromic diseases may not respond to AONs or variant specific gene editing, it is important to investigate the potential of novel approaches with a broader range of action.

Flavonoids are plant-derived small molecules that can influence synaptic plasticity and potentially exert cognitive benefits (14–16). A phenotype-based screen of compounds that could restore ciliation and cilium length in CEP290^{null} RPE1 cells identified the flavonoid eupatilin (5,7-dihydroxy-3',4',6-trimethoxyflavone) as a candidate therapeutic molecule for retinal ciliopathies (17). Treatment of the rd16 *Cep290* mouse model of retinal dystrophy showed increased photopic responses and improved M-opsin immunofluorescence in the outer retina, although no effect on rhodopsin traffic or rod cell function were reported (17). Eupatilin was also reported to rescue ciliary gating in the absence of Rpgrip1l (nphp8) in mouse embryonic fibroblasts (18). Both CEP290 and RPGRIP1L are part of the ciliary transition zone (TZ), a cilia domain distal to the basal body that functions as a gatekeeper of cilia protein import and export (19–21). Eupatilin has previously been used in the clinic as a drug treatment for gastritis and peptic ulcer with reportedly limited adverse effects (22).

In this study, we investigated the effect of eupatilin in different models of human *CEP290* disease, including patient-derived fibroblasts, CRISPR-induced RPE1 knockout cells, and induced pluripotent stem cell (iPSC)-derived retinal organoids, thus, evaluating its potential as a variant-independent therapeutic approach for the treatment of ciliopathies.

Results

Eupatilin increases cilia incidence and length in CEP290 LCA10 patient fibroblasts

Dermal fibroblasts derived from an affected male individual with LCA10 and homozygous for the *CEP290* c.2991+1655A>G variant were compared to fibroblasts from a control individual (**Figure 1**). Ciliation was induced and evaluated by immunocytochemistry (**Figure 1A**). CEP290 LCA10 fibroblasts displayed reduced cilia incidence (**Figure 1B**) and the cilia present were reduced in length (**Figure 1C**), confirming previously reported results (23). Importantly, treatment with 20 μM eupatilin significantly increased cilia incidence (**Figure 1B**) and rescued cilia length in CEP290 LCA10 patient fibroblasts (**Figure 1C**), whilst having no significant effect in controls.

Eupatilin restores cilia incidence and length in CEP290 knockout RPE1 cells

In order to validate the reported effects of eupatilin on RPE1 cilia, we made an independent *CEP290* knockout (KO) cell line using CRISPR/Cas9 gene editing (**Figure 2**). A guide RNA (gRNA) in exon 6 was used to direct Cas9 to cleave *CEP290*. RPE1 clones were selected and screened for insertions or deletions (InDels) resulting in frame shifts. An RPE1 cell line was selected with a homozygous 1 bp deletion (c.C311del; p.Ser104Leufs*20) that leads to a frame shift (at amino acid 104) and a premature stop codon after 20 amino acids similar to a pathogenic variant reported in Joubert and Meckel-Gruber syndromes (c.338T>A: p.Leu113*), and as such is predicted to be a severe 'null' mutation (**Figure 2A**). Characterization of this cell line showed that the expression of *CEP290* transcript was reduced by 80%, presumably due to nonsense mediated decay (**Figure 2B**) and protein expression was reduced to 20% of isogenic control level (**Figure 2C,D**). Exon 6 is in-frame with exon 5 and exon 7, leading to the possibility of exon 6 skipping producing a truncated protein, lacking the 48 amino acids of exon 6 and giving rise to the band detected by immunoblotting. It is not known if this truncated form of CEP290 is functional; however, no CEP290 protein could be detected at the basal body of the CEP290 KO cells by immunocytochemistry, unlike in the isogenic control RPE1 cells (**Supplementary Figure 1**).

The *CEP290* KO RPE1 cells showed significant reductions in both cilia incidence and cilia length (**Figure 2E-G**), i.e. fewer and shorter cilia. Importantly, treatment with 20 μM eupatilin led to a significant increase in cilia incidence and length, returning to similar levels as the isogenic control cell line (**Figure 2E-G**). Interestingly, eupatilin treatment also led to a small, but significant, increase in cilia length in control RPE1 cells.

A more detailed investigation of the effect of eupatilin on cilia incidence and length in CEP290 KO RPE1 cells revealed that there was a dose response for the effect of eupatilin on cilia length and incidence (**Figure 2H,I**), 5 μM eupatilin resulted in a small increase in cilia incidence and length, which did not reach statistical significance. By contrast, both 10 μM and 20 μM eupatilin led to statistically significant increases in cilia incidence and length with 20 μM eupatilin restoring incidence and length to isogenic control levels (dashed red line).

Eupatilin treatment restores ciliation and cilia length in iPSC-derived CEP290 LCA10 and CEP290 KO retinal organoids

CEP290 KO iPSC were developed in a control line by CRISPR/Cas9 technology and the same guide RNA used for the CEP290 KO RPE1 cell line. An iPSC line with compound heterozygous single base pair deletions (c.C315del and c.T316del alleles; p.Ser104Leufs*20) was selected (**Supplementary Figure 1**). This iPSC line is predicted to cause the same frame shift and premature stop codon as the CEP290 KO RPE1 cells. CEP290 immunoreactivity was undetectable at the cilia of these iPSC, in contrast to control iPSC, similar to the CEP290

KO RPE1 cells (**Supplementary Figure 1**). CEP290 LCA10 fibroblasts reprogrammed to iPSC (8,23) were differentiated to retinal organoids together with the CEP290 KO iPSC line, as previously described (24). The CEP290 LCA10 and CEP290 KO iPSC produced retinal organoids with a characteristic neuroepithelial morphology that were similar to control organoids (CEP290 WT) early in development (**Figure 3A**). Photoreceptor differentiation was confirmed through cone-rod homeobox (CRX) and recoverin (RCVRN) immunoreactivity in the outer nuclear layer after 120 days of differentiation (D120) (**Figure 3B**). CEP290 staining confirmed the absence of CEP290 protein in both CEP290 KO and CEP290 LCA10 retinal organoids (**Supplementary Figure 2**). Treatment with eupatilin was initiated at 90 days of differentiation (D90), after polarized organization of photoreceptors has occurred, and continued for 30 days before harvesting for analyses of cilia morphology by immunohistochemistry (IHC) at D120. CEP290 LCA10 retinal organoids showed reduced cilia incidence and cilia length, as previously reported (8,23,25). The CEP290 KO retinal organoids also had reduced cilia incidence and shorter cilia than the control organoids, and were comparable with the CEP290 LCA10 organoids (**Figure 3C-E**). Importantly, treatment with eupatilin at 10 or 20 μM led to significant increases in cilia incidence and length in both CEP290 KO and CEP290 LCA10 retinal organoids (**Figure 3D,E**).

Opsin accumulates in the outer nuclear layer of CEP290 LCA10 retinal organoids and is rescued by eupatilin

To test the effect of eupatilin on outer segment protein traffic, we compared opsin localization in CEP290 LCA10 and control retinal organoids at D180. Staining for rhodopsin (RHO) and L/M opsin suggested that there was retention of rhodopsin in the outer nuclear layer (ONL) of the CEP290 LCA10 organoids at D180, compared to control organoids (**Figure 4A,B**). L/M opsin was equally accumulated in the ONL of controls and CEP290 LCA10 organoids (**Figure 4A,B).** Interestingly, treatment with 20 μM eupatilin for 30 days (D150 to D180) reduced the accumulation of rhodopsin and L/M opsin within the ONL (**Figure 4A,B**).

Eupatilin treatment reduces the expression of rhodopsin

To determine the potential mechanisms related to the decrease in rhodopsin in the ONL, we performed qPCR analyses on mature (D250) control organoids that had been treated with eupatilin for 30 days (**Figure 5A**). These analyses revealed that eupatilin treatment caused a significant reduction of over 50% in *RHO* expression at 10 μM. The 20 μM treatment also reduced *RHO* transcript, but did not reach statistical significance **(Figure 5A)**. The expression changes in other photoreceptor genes were less pronounced, and only *CRX* was significantly reduced at 10 μM. Both *OPN1MW/OPN1LW* and *ARR3* showed a trend for reduced expression, although not significantly, suggesting a potential effect on cones as well as rods **(Figure 5A)**. The effect of eupatilin on *RHO* and other photoreceptor transcript levels appeared to be transient, however, as the levels were restored to control levels when the samples were allowed to recover for 14 days after 10 μM and 20 μM eupatilin treatment **(Figure 5A)**.

Eupatilin modulates the expression of ciliary and synaptic pathways

To assess the effect of eupatilin on global retinal transcription, we performed bulk RNA sequencing (RNAseq) on mature control organoids treated with 20 μM eupatilin for 30 days from D210 to D240 (**Figure 5B-E**). Clustering of the samples by significant differential expression showed that the eupatilin treated samples had similar expression patterns, distinct from the vehicle treated samples (**Figure 5B**). Out of 56,558 mapped genes, 645 genes were differentially expressed with 461 downregulated genes and 184 upregulated genes identified at false discovery rate (FDR)-adjusted p-value cutoff of 0.1 (Figure 5C). Filtered by adjusted

p-values, the most significantly downregulated genes were *PRR15*, a gene with unknown function but exclusively expressed in post-mitotic cells; *NRXN3*, a presynaptic adhesion molecule that regulates neurotransmitter release (26); the cone photoreceptor kinase *GRK7* that catalyzes phosphorylation of cone opsins (27) and *TENM2*, a receptor involved in calcium mediated signaling in synapses (28). The most significantly upregulated gene was the heat shock response gene *HSPA6*, which encodes an inducible Hsp70 protein (**Figure 5C**). Over-representation analysis revealed two major set of genes transcriptionally affected by eupatilin: one involving photoreceptor neuron synapse genes, and one involving cilia genes (**Figure 5D**). Interestingly, eupatilin altered the expression of essential phototransduction genes involved in several forms of retinal degeneration, including *CRB1*, *EYS*, *SAG*, *GRK7*, *RPGRIP1*, *USH2A*, *PROM1*, *ARR3*, *PDC*, *PDE6A*, *GNGT1*, *GUCA1C*; the photoreceptor cation channels *CNGA1* and *CNGB1*; and the cilia transmembrane protein genes *PKHD1*, *PKD2L1*, *PCDHB15*, *CDH23* (*USH1D*) and *PCDH15* (*USH1F*) (**Figure 5E**). *RHO* expression was also reduced, although it did not reach statistical significance (p-value=0.258, not shown).

Discussion

Leber Congenital Amaurosis type 10 (LCA10) is a severe retinal disease caused by biallelic variants in the ciliary gene *CEP290*. Despite the recent clinical trials of gene-editing and RNA-targeted therapies (8–12,29,30), effective treatments are still limited. Plant flavonoid supplementation is being studied for the treatment for a range of different ocular disorders (31). For example, baicalein has been found to lower intraocular pressure in glaucoma (32) by regulating PI3K/AKT signalling (33), while quercetin provides neuroprotective effects in diabetic rat retinas (34) and in mouse models of light-induced retinal degeneration (35).

Eupatilin (5,7-dihydroxy-3',4',6-trimethoxyflavone) is a flavone derived from the plant genus *Artemisia* with different anti-oxidant (36,37), anti-ulcerative (38), anti-cancer (39,40) and anti-inflammatory (41,42) properties (43). Eupatilin is prescribed clinically in South Korea for the treatment of gastritis and peptic ulcers under the name of Stillen^{TM} (44). Previously, it has been reported that eupatilin can rescue cilia defects due to the absence of CEP290 in RPE1 CEP290^{null} cells (17). In addition, eupatilin helped to rescue cilia TZ defects in *Rpgrip1l*$^{-/-}$ mouse embryonic fibroblasts (18). CEP290 and RPGRIP1L are both TZ proteins important for regulating the entry and exit of proteins to cilia (19). In the retina, CEP290 is required for RPE maturation and functional polarization (45), as well as for photoreceptor ciliogenesis (46). In RPE and other primary cilia, CEP290 localises to the TZ, but in photoreceptors, CEP290 localises along the length of the connecting cilium (47) and follows a 9-fold symmetry close to the Y-links (48). This supports a role for CEP290 in photoreceptor cilia different from other primary cilia.

The aim of this study was to validate and extend the previous report by Kim and colleagues (17) on the effect of eupatilin as a variant-independent approach to treat CEP290 ciliary disease. We confirmed the beneficial effect on ciliation and cilium length in a newly generated CRISPR/Cas9 CEP290 KO RPE1 cell line. We also demonstrated this beneficial effect in CEP290 LCA10 patient fibroblasts. This effect of eupatilin was dose-dependent, with 10 and 20 μM being most beneficial in RPE1 cells. This dose-dependent effect has been reported with ciliation rescue plateauing with concentrations above 20 μM in cells, and 40 mg/kg being sufficient for opsin rescue in the mouse retina (17). Furthermore, we show that eupatilin can also rescue photoreceptor cilia defects in CEP290 KO and CEP290 LCA10 iPSC-derived retinal organoids.

We have previously reported that patient derived CEP290 LCA10 fibroblasts present ciliation and cilium length defects (23). These defects are caused by the inclusion of a cryptic exon in CEP290 between exons 26 and 27 that causes reduced CEP290 expression (40-50% of control) in fibroblasts and delays in ciliation, whereas there is little (10-20%) correctly spliced CEP290 expression in retinal organoids (23). Similarly, we show that CEP290 KO RPE1 cells have reduced CEP290 expression (10-20% of control), but not total ablation, potentially due to partial exon 6 skipping and production of an in-frame truncated protein (49). We have identified a potentially important phenotype in CEP290 LCA10 retinal organoids: the accumulation of visual opsins in the outer nuclear layer of photoreceptors, which is reduced by eupatilin. We also show that eupatilin modulates gene transcription to reduce *RHO* expression. This reduction of *RHO* expression might be responsible for the observed reduced rhodopsin ONL accumulation. Thus, reducing the burden of cilia traffic in a ciliopathy could be beneficial and might also assist the transport of the remaining protein. Our observations contrast with previous work in mice by Kim and colleagues, where they observed a rescue of cone opsins in the outer segments, but no changes in rhodopsin. Differences between murine and human models may play a role in this discrepancy, especially taking in consideration the

differences in photoreceptor composition and splicing mechanisms between human and mouse (50).

Eupatilin was suggested to exert its effect on CEP290 ciliopathy at the protein level through calmodulin binding and release of NPHP5 to the transition zone (17). In NPHP5 LCA5 retinal organoids, CEP290 expression is reduced, and rhodopsin mislocalises to the ONL. In contrast to CEP290, NPHP5 LCA patient fibroblasts and iPSC-RPE present abnormally long cilia (51), similar to what was reported in RPGRIP1L KO cells (18). This could be explained by aberrant cargo transport of ciliary proteins due to reduced CEP290. The depletion of CEP290 affects the cilium in a different way than the absence of NPHP5 or RPGRIP1L, since it interferes with the ciliary microtubule organization, thus reducing ciliation and cilium length (52).

Calmodulin is a Ca^{2+} binding protein that interacts with other centrosomal proteins with Ca^{2+} binding properties such as centrin, CEP110 (a CEP290 interactor) or CEP97 (53–56). In photoreceptors, calmodulin acts by regulating calcium storage in phototransduction (57). Eupatilin could be acting therefore at different levels in the photoreceptor cell, in the outer segments and at the cilia base. We did not observe changes in the expression levels of *CALM1* which encodes calmodulin, in the RNAseq data; however, some Ca^{2+}-related genes similar to calmodulin, like calcium-binding protein 1 (*CABP1*), *CABP4*, *CAMK4*, *CADPS*, and *CALB1*, were downregulated. The calcium-binding protein DREAM, from the recoverin family, functions as a calcium-regulated transcriptional repressor (58,59) and its modulation could have therapeutic potential for neurological diseases such as Alzheimer's disease (60). This suggests that targeting calcium signalling pathways with compounds like eupatilin could be useful for modulating other neurodegenerative diseases.

RNAseq analysis also revealed that eupatilin downregulated two major gene modules: one involving neural synapse genes (e.g., *TENM2*, *NRXN3*) and a second module involving photoreceptor cilia genes (e.g., *EYS*, *RPGRIP1*, *USH2A*, *PROM1*, *PKHD1*, *ARR3*, *GRK7*, *RRH*, *SAG*, *PDE6A*, *CNGA1*). The effect of eupatilin at the transcriptional level on phototransduction or outer segment genes has not been reported before. Studying the interaction of eupatilin with cilia genes in more detail might reveal other potential and more specific targets that could be used to treat CEP290 related disease. Some studies suggest a role of flavonoids in modulating synaptic plasticity (61), but the precise role and the mechanisms by which flavonoids modulate cognitive functions are yet to be fully established (62,63).

While most of the transcriptional effects of eupatilin appear to be downregulation, some genes were upregulated by eupatilin. The most significantly upregulated gene was the heat-shock response gene *HSPA6*, while *HSPA12A* was also upregulated, suggesting that eupatilin might activate the heat shock response. In certain models of retinal degeneration, *HSPA1A* overexpression is thought to play a protective role in stressed photoreceptors (64,65). For instance, *HSPA6* and *HSPA1A* contribute to protection of differentiated human neuronal cells from cellular stress (66,67). However, the role of *HSPA6* and *HSPA12A* in photoreceptors is still not known. Future studies could investigate the transcriptional effect of eupatilin in CEP290 LCA10 retinal organoids to better understand CEP290 retinal disease, while scRNA sequencing could help understand the impact of eupatilin on the different retinal cell populations.

In summary, we have confirmed the beneficial effect of eupatilin on different CEP290 ciliopathy models, including CEP290 retinal organoids. We also provide novel insights into the effect of eupatilin at the transcriptional level in control retinal organoids. Taken together, this work supports eupatilin as a potential variant-independent approach for CEP290-associated ciliopathies.

Methods

Cell lines

hTert-RPE1 control cells were a kind gift from Ronald Roepman (Radboud University Nijmegen, The Netherlands). Guide RNAs (gRNAs) were designed to target CEP290 exon 6 and cloned into the pSpCas9(BB)-2A-GFP (PX458; gift from Feng Zhang; Addgene plasmid #48138). RPE1 cells were transfected with this plasmid by using Lipofectamine 3000 (Invitrogen). Transfected cells were subjected to puromycin selection after transfection and subsequently seeded as single cells into 96-multiwell plates in order to screen for CEP290 KO clones. CEP290 LCA10 patient fibroblasts and iPSC used in this work were characterized in Parfitt et al. (23).

Isogenic CEP290 KO stem cells were generated (68), using a simultaneous cellular reprogramming and CRISPR/Cas9 gene editing protocol (69), by targeting CEP290 exon 6 in otherwise healthy human dermal fibroblasts, of neonatal origin (HDFn). Control HDFn cells were Nucleofected using Cell Line Nucleofector Kit R (Lonza) containing 1µg of each episomal reprogramming vector (70) and 1µg of the CEP290 targeting PX458 plasmid.

Following nucleofection, cultures were maintained until the presence of iPSC colonies emerged. Individual clones were mechanically isolated and placed into individual wells of a geltrex-coated 12-well plate. Clonal iPSC lines were subsequently amplified, before DNA extraction using the Wizard SV genomic DNA extraction kit (Promega) following the manufacturer's instructions. The CRISPR/Cas9 target region was expanded using standard PCR and analysed by Sanger sequencing to detect the presence or absence of CRISPR/Cas9 induced variants by aligning the sample sequence data to the CEP290 reference sequence (ENST00000552810, ensembl.org) on Benchling (Benchling.com).

Control iPSC were produced as previously described (71).

qPCR

Total RNA was extracted using the RNeasy Mini Kit (QIAGEN) following the manufacturer's instructions. First strand cDNA synthesis was performed using the Tetro cDNA synthesis kit (Bioline). Quantitative PCR (qPCR) was completed using the SYBR green method carried out on a QuantStudio 6 Flex Real-Time PCR System (Applied Biosystems) using LabTaq Green Hi Rox (Labtech). Primers are listed in **Supplementary Table 1**. Relative gene expression levels were determined using the ΔΔCt method, using the geometric mean of *GAPDH* and *ACTIN* as the reference. GraphPad Prism v.8 (GraphPad Software, Inc.) was used for statistical analyses and generating plots.

Western blot

Total protein samples were lysed in radioimmunoprecipitation (RIPA) buffer containing 2% protease inhibitor cocktail (Sigma). Protein quantification was completed using the Pierce Bicinchoninic acid (BCA) Protein Assay (ThermoFisher) following the manufacturers microplate procedure. Equal amounts of protein were run on 8% acrylamide gels before protein transfer to nitrocellulose membranes via wet transfer. Protein membranes were incubated with primary antibodies for CEP290 or relevant reference proteins overnight at 4°C before incubation with HRP-conjugated secondary antibodies. Finally, protein was detected using Clarity Western ECL substrate (BioRad) and imaged with ImageLab on a BioRad ChemiDoc XRS+. Quantification of western blots was performed with ImageLab software (bio-rad.com) and target protein expression was normalized to reference proteins before analysis.

Immunocytochemistry

hTERT-RPE1, fibroblasts or iPSC were grown on chamber slides until 90% confluency was reached. To induce cilia growth, fibroblasts and hTERT-RPE1 cells were incubated with serum starvation medium (DMEM/F12, 0.2% FBS + 1% Pen/Strep + 1% Sodium pyruvate), while iPSC were cultured as normal with mTESR Plus medium.

Twenty-four hours post-starvation, cultured cells were fixed in 2% paraformaldehyde (PFA) for 15 min at room temperature (RT), followed by 1% Triton-X-100 treatment for 5 min and blocking in 2% Fetal bovine serum (FBS) for 20 minutes. Subsequently, cells were incubated with primary antibodies diluted in blocking solution for 1 hour. After incubation, cells were washed three times in phosphate buffered saline (PBS) and incubated with the corresponding Alexa Fluor conjugated secondary antibody (ThermoFisher). After secondary antibody incubation, DAPI (ThermoFisher) was incubated for 5 min. Finally, slides were washed three times in PBS for 5 minutes and mounted in DAKO fluorescence mounting medium (Agilent).

iPSC differentiation to retinal organoids

iPSC were differentiated to retinal organoids as previously described (24) with small variations. Briefly, cells were seeded on Geltrex-coated (Thermo Fisher) six-well plates with mTESR Plus Medium (Stem Cell Technologies) until 90-95% confluency. Essential 6™ Medium (Thermo Fisher) was added to the culture for 2 days followed by addition of neural induction media (Advanced DMEM/F-12 (1:1), 1% N2 supplement, 2 mM GlutaMax, 1% Pen/Strep) until neuro retinal vesicles (NRVs) appeared. On day 6 of differentiation, a single treatment with 1.5 nM BMP4 (Prepotech) was added, and half media changes were carried out until day 16. NRVs were excised and kept in ultra-low binding 96-well plates for maturation. For retinal differentiation and maturation, serum-free retinal differentiation media was added (DMEM/F12 (3:1), 2% B27, 1% non-essential amino-acids, 1% Pen/Strep) for 6 days after collection. For retinal maturation, media was supplemented with 10% FBS, 100 µM Taurine and 2mM GlutaMax. Retinoic acid (1 µM) was added on day 50. On day 70, N2 was added to the media (RMM2), and the concentration of retinoic acid was reduced to 0.5 µM. To promote photoreceptor differentiation, retinoic acid was removed from the media on day 100.

Cryopreservation and immunohistochemistry of retinal organoids

Retinal organoids were briefly washed once in PBS and placed in a mixture of 4% PFA + 5% sucrose in PBS for 40 minutes. Organoids were then placed in 6.25% sucrose in PBS for 1 hour, followed by 12.5% sucrose in PBS for 30 minutes and in 25% sucrose in PBS for 1 hour. All incubation steps were performed at 4°C. Organoids were then embedded in OCT, slowly frozen on dry ice, and stored at -80°C until cryosectioning. Cryosections (7 µm thick) were collected and stored at -20°C for later analysis.

For immunohistochemistry, sections were first washed once in PBS and blocked with 10% donkey serum, 0.05% Triton X-100 in PBS for 30 minutes. Primary antibodies used were the following: anti-rabbit CEP290 (Abcam) ab84870, 1:100; anti-rabbit ARL13B (Proteintech) 1:1000; anti-mouse Pericentrin (Abcam) ab28144, 1:1000; anti-mouse Rhodopsin 4D2 (Millipore) MABN15 1:1000; anti-rabbit Opsin Antibody, Red/Green (Millipore) 1:500; anti-mouse CRX (Abnova) H00001406-M02 1:1000; anti-rabbit Recoverin (Millipore) AB5585 1:1000. Primary antibodies were incubated in the blocking solution diluted 50% in PBS for 1 hour. Sections were then washed in PBS and incubated with Alexa Fluor (Thermo Fisher) secondary antibodies in the diluted blocking solution for 45 minutes. Nuclei were visualized using DAPI (2 µg/mL). Samples were washed in PBS and mounted using DAKO fluorescence mounting medium (Agilent).

Cilia quantification and statistical analysis

Images were obtained using a Carl Zeiss LSM700 laser-scanning confocal microscope, or a Leica Stellaris 8 confocal microscope. At least 3 images were taken for each condition. Cilia were segmented and cilium length was quantified using the plugin CiliaQ on Fiji/ImageJ based on the ARL13B channel (and basal body present in the PCN channel) (66). Manual counting was done to measure photoreceptor ciliation and cilia length in Figure 3D,E. Statistical analyses were done using Prism and are indicated at the bottom of each figure legend.

RNAseq pre-processing and analysis

Total RNA was extracted with the RNeasy micro kit (QIAGEN) following the manufacturer's instructions.

The Illumina NovaSeq platform was used to obtain raw sequencing data which was subjected to quality control using FastQC. Trimmomatic was used to remove any low-quality sequences, adapter sequences and other contaminants. Trimmed reads were aligned to the GRCh38 reference genome using the STAR aligner. Gene expression was quantified using the featureCounts program.

The gene-level count data was imported into RStudio for differential gene expression analysis using the DESeq2 package (72). The gene counts were normalized using the DESeq2 normalization method, which accounts for differences in library size and gene length. A generalised linear model was fitted to the normalized counts using the negative binominal distribution. The differential gene expression analysis was carried out using the DESeq2 function with apeglm shrinkage (73). Genes with an FDR-adjusted p value cutoff of 0.1 were considered significant. An over-representation analysis was carried out using the clusterProfiler package for identification of cellular components enriched in the significantly differentially expressed gene-set.

Acknowledgments and funding

This work was supported by the Foundation Fighting Blindness (USA), Moorfields Eye Charity, RetinaUK, Fight for Sight (UK) and The Wellcome Trust. We are thankful to Prof. Ronald Roepman for providing the hTert-RPE1 control cells.

Author contributions

BCM and MEC conceived the study. MEC directed the project. JCCS, PES, DO and DA conducted the experiments involving fibroblasts, RPE1 and retinal organoids. KJ and DO helped with the CRISPR-Cas9 design. FOR and JvdS helped with the transcriptomic analyses. JCCS, PES and MEC wrote the paper. All authors edited the draft manuscript.

References

1. Sayer, J.A., Otto, E.A., O'Toole, J.F., Nurnberg, G., Kennedy, M.A., Becker, C., Hennies, H.C., Helou, J., Attanasio, M., Fausett, B. v., *et al.* (2006) The centrosomal protein nephrocystin-6 is mutated in Joubert syndrome and activates transcription factor ATF4. *Nat Genet*, **38**, 674–681.

2. Valente, E.M., Silhavy, J.L., Brancati, F., Barrano, G., Krishnaswami, S.R., Castori, M., Lancaster, M.A., Boltshauser, E., Boccone, L., Al-Gazali, L., *et al.* (2006) Mutations in CEP290, which encodes a centrosomal protein, cause pleiotropic forms of Joubert syndrome. *Nat Genet*, **38**, 623–625.

3. Rachel, R.A., Li, T. and Swaroop, A. (2012) Photoreceptor sensory cilia and ciliopathies: focus on CEP290, RPGR and their interacting proteins. *Cilia*, **1**.

4. den Hollander, A.I., Koenekoop, R.K., Yzer, S., Lopez, I., Arends, M.L., Voesenek, K.E.J., Zonneveld, M.N., Strom, T.M., Meitinger, T., Brunner, H.G., *et al.* (2006) Mutations in the CEP290 (NPHP6) Gene Are a Frequent Cause of Leber Congenital Amaurosis. *Am J Hum Genet*, **79**, 556.

5. Coppieters, F., Lefever, S., Leroy, B.P. and de Baere, E. (2010) CEP290, a gene with many faces: mutation overview and presentation of CEP290base. *Hum Mutat*, **31**, 1097–1108.

6. Garanto, A., Chung, D.C., Duijkers, L., Corral-Serrano, J.C., Messchaert, M., Xiao, R., Bennett, J., Vandenberghe, L.H. and Collin, R.W.J. (2016) In vitro and in vivo rescue of aberrant splicing in CEP290-associated LCA by antisense oligonucleotide delivery. *Hum Mol Genet*, **25**, 2552–2563.

7. Maeder, M.L., Stefanidakis, M., Wilson, C.J., Baral, R., Barrera, L.A., Bounoutas, G.S., Bumcrot, D., Chao, H., Ciulla, D.M., DaSilva, J.A., *et al.* (2019) Development of a gene-editing approach to restore vision loss in Leber congenital amaurosis type 10. *Nature Medicine 2019 25:2*, **25**, 229–233.

8. Dulla, K., Aguila, M., Lane, A., Jovanovic, K., Parfitt, D.A., Schulkens, I., Chan, H.L., Schmidt, I., Beumer, W., Vorthoren, L., *et al.* (2018) Splice-Modulating Oligonucleotide QR-110 Restores CEP290 mRNA and Function in Human c.2991+1655A>G LCA10 Models. *Mol Ther Nucleic Acids*, **12**, 730–740.

9. Russell, S.R., Drack, A. v., Cideciyan, A. v., Jacobson, S.G., Leroy, B.P., van Cauwenbergh, C., Ho, A.C., Dumitrescu, A. v., Han, I.C., Martin, M., *et al.* (2022) Intravitreal antisense oligonucleotide sepofarsen in Leber congenital amaurosis type 10: a phase 1b/2 trial. *Nature Medicine 2022 28:5*, **28**, 1014–1021.

10. Cideciyan, A. V., Jacobson, S.G., Ho, A.C., Garafalo, A. V., Roman, A.J., Sumaroka, A., Krishnan, A.K., Swider, M., Schwartz, M.R. and Girach, A. (2021) Durable vision improvement after a single treatment with antisense oligonucleotide sepofarsen: a case report. *Nature Medicine 2021 27:5*, **27**, 785–789.

11. Cideciyan, A. V., Jacobson, S.G., Drack, A. V., Ho, A.C., Charng, J., Garafalo, A. V., Roman, A.J., Sumaroka, A., Han, I.C., Hochstedler, M.D., *et al.* (2019) Effect of an intravitreal antisense oligonucleotide on vision in Leber congenital amaurosis due to a photoreceptor cilium defect. *Nat Med*, **25**, 225–228.

12. Cideciyan, A. V., Jacobson, S.G., Ho, A.C., Krishnan, A.K., Roman, A.J., Garafalo, A. V., Wu, V., Swider, M., Sumaroka, A., Van Cauwenbergh, C., *et al.* (2022) Restoration

of Cone Sensitivity to Individuals with Congenital Photoreceptor Blindness within the Phase 1/2 Sepofarsen Trial. *Ophthalmology Science*, **2**, 100133.

13. ProQR Therapeutics N.V. (2022) ProQR Announces Additional Sepofarsen Illuminate Trial Analyses and Provides Update on Company Strategy. *ProQR Announces Additional Sepofarsen Illuminate Trial Analyses and Provides Update on Company Strategy*; (2022) .

14. Kennedy, D.O. (2014) Polyphenols and the Human Brain: Plant "Secondary Metabolite" Ecologic Roles and Endogenous Signaling Functions Drive Benefits. *Advances in Nutrition*, **5**, 515–533.

15. Rendeiro, C., Foley, A., Lau, V.C., Ring, R., Rodriguez-Mateos, A., Vauzour, D., Williams, C.M., Regan, C. and Spencer, J.P.E. (2014) A role for hippocampal PSA-NCAM and NMDA-NR2B receptor function in flavonoid-induced spatial memory improvements in young rats. *Neuropharmacology*, **79**, 335–344.

16. Williams, C.M., el Mohsen, M.A., Vauzour, D., Rendeiro, C., Butler, L.T., Ellis, J.A., Whiteman, M. and Spencer, J.P.E. (2008) Blueberry-induced changes in spatial working memory correlate with changes in hippocampal CREB phosphorylation and brain-derived neurotrophic factor (BDNF) levels. *Free Radic Biol Med*, **45**, 295–305.

17. Kim, Y.J., Kim, S., Jung, Y., Jung, E., Kwon, H.J. and Kim, J. (2018) Eupatilin rescues ciliary transition zone defects to ameliorate ciliopathy-related phenotypes. *Journal of Clinical Investigation*, **128**, 3642–3648.

18. Wiegering, A., Dildrop, R., Vesque, C., Khanna, H., Schneider-Maunoury, S. and Gerhardt, C. (2021) Rpgrip1l controls ciliary gating by ensuring the proper amount of Cep290 at the vertebrate transition zone. *Mol Biol Cell*, **32**, 675–689.

19. Garcia-Gonzalo, F.R., Corbit, K.C., Sirerol-Piquer, M.S., Ramaswami, G., Otto, E.A., Noriega, T.R., Seol, A.D., Robinson, J.F., Bennett, C.L., Josifova, D.J., *et al.* (2011) A transition zone complex regulates mammalian ciliogenesis and ciliary membrane composition. *Nature Genetics 2011 43:8*, **43**, 776–784.

20. Wu, Z., Pang, N., Zhang, Y., Chen, H., Peng, Y., Fu, J. and Wei, Q. (2020) CEP290 is essential for the initiation of ciliary transition zone assembly. *PLoS Biol*, **18**.

21. Jensen, V.L., Li, C., Bowie, R. v, Clarke, L., Mohan, S., Blacque, O.E. and Leroux, M.R. (2015) Formation of the transition zone by Mks5/Rpgrip1L establishes a ciliary zone of exclusion (CIZE) that compartmentalises ciliary signalling proteins and controls PIP2 ciliary abundance. *EMBO J*, **34**, 2537–2556.

22. Ryoo, S.B., Oh, H.K., Yu, S.A., Moon, S.H., Choe, E.K., Oh, T.Y. and Park, K.J. (2014) The Effects of Eupatilin (Stillen®) on Motility of Human Lower Gastrointestinal Tracts. *Korean J Physiol Pharmacol*, **18**, 383.

23. Parfitt, D.A., Lane, A., Ramsden, C.M., Carr, A.J.F., Munro, P.M., Jovanovic, K., Schwarz, N., Kanuga, N., Muthiah, M.N., Hull, S., *et al.* (2016) Identification and Correction of Mechanisms Underlying Inherited Blindness in Human iPSC-Derived Optic Cups. *Cell Stem Cell*, **18**, 769–781.

24. Corral-Serrano, J.C., Lamers, I.J.C., Van Reeuwijk, J., Duijkers, L., Hoogendoorn, A.D.M., Yildirim, A., Argyrou, N., Ruigrok, R.A.A., Letteboer, S.J.F., Butcher, R., *et al.* (2020) PCARE and WASF3 regulate ciliary F-actin assembly that is required for the

initiation of photoreceptor outer segment disk formation. *Proc Natl Acad Sci U S A*, **117**, 9922–9931.

25. Shimada, H., Lu, Q., Insinna-Kettenhofen, C., Nagashima, K., English, M.A., Semler, E.M., Mahgerefteh, J., Cideciyan, A. v., Li, T., Brooks, B.P., *et al.* (2017) In Vitro Modeling Using Ciliopathy-Patient-Derived Cells Reveals Distinct Cilia Dysfunctions Caused by CEP290 Mutations. *Cell Rep*, **20**, 384–396.

26. Hishimoto, A., Pletnikova, O., Lang, D.L., Troncoso, J.C., Egan, J.M. and Liu, Q.R. (2019) Neurexin 3 transmembrane and soluble isoform expression and splicing haplotype are associated with neuron inflammasome and Alzheimer's disease. *Alzheimers Res Ther*, **11**, 1–15.

27. Chen, Mol Vis 2001; 7:305-313. http://www.molvis.org/molvis/v7/a43/ (accessed Sep 2, 2022).

28. Silva, J.-P., Lelianova, V.G., Ermolyuk, Y.S., Vysokov, N., Hitchen, P.G., Berninghausen, O., Rahman, M.A., Zangrandi, A., Fidalgo, S., Tonevitsky, A.G., *et al.* Latrophilin 1 and its endogenous ligand Lasso/ teneurin-2 form a high-affinity transsynaptic receptor pair with signaling capabilities. .

29. Ramsbottom, S.A., Molinari, E., Srivastava, S., Silberman, F., Henry, C., Alkanderi, S., Devlin, L.A., White, K., Steel, D.H., Saunier, S., *et al.* (2018) Targeted exon skipping of a CEP290 mutation rescues Joubert syndrome phenotypes in vitro and in a murine model. *Proc Natl Acad Sci U S A*, **115**, 12489–12494.

30. Editas Medicine Announces Clinical Data Demonstrating Proof of Concept of EDIT-101 from Phase 1/2 BRILLIANCE Trial (2022) .

31. Davinelli, S., Ali, S., Scapagnini, G. and Costagliola, C. (2021) Effects of Flavonoid Supplementation on Common Eye Disorders: A Systematic Review and Meta-Analysis of Clinical Trials. *Front Nutr*, **8**, 264.

32. Li, H.L., Ashpole, N.E., Navarro, I.D., Lam, T.C., Chan, H.L.H., To, C.H., Stamer, W.D. and Do, C. (2015) Baicalein lowers intraocular pressure and increases outflow facility in mouse eye. *Invest Ophthalmol Vis Sci*, **56**, 4853–4853.

33. Zhao, N., Shi, J., Xu, H., Luo, Q., Li, Q. and Liu, M. (2021) Baicalin suppresses glaucoma pathogenesis by regulating the PI3K/AKT signaling in vitro and in vivo. *https://doi.org/10.1080/21655979.2021.2001217*, **12**, 10187–10198.

34. Ola, M.S., Ahmed, M.M., Shams, S. and Al-Rejaie, S.S. (2017) Neuroprotective effects of quercetin in diabetic rat retina. *Saudi J Biol Sci*, **24**, 1186.

35. Ortega, J.T., Parmar, T., Golczak, M. and Jastrzebska, B. (2021) Protective effects of flavonoids in acute models of light-induced retinal degeneration. *Mol Pharmacol*, **99**, 60–77.

36. Jegal, K.H., Ko, H.L., Park, S.M., Byun, S.H., Kang, K.W., Cho, I.J. and Kim, S.C. (2016) Eupatilin induces Sestrin2-dependent autophagy to prevent oxidative stress. *Apoptosis*, **21**, 642–656.

37. Lee, M., Yang, C., Song, G. and Lim, W. (2021) Eupatilin Impacts on the Progression of Colon Cancer by Mitochondria Dysfunction and Oxidative Stress. *Antioxidants*, **10**.

38. Huh, K., Kwon, T.H., Shin, U.S., Kim, W.B., Ahn, B.O., Oh, T.Y. and Kim, J.A. (2003) Inhibitory effects of DA-9601 on ethanol-induced gastrohemorrhagic lesions and gastric xanthine oxidase activity in rats. *J Ethnopharmacol*, **88**, 269–273.

39. Kim, M.J., Kim, D.H., Na, H.K., Oh, T.Y., Shin, C.Y. and Surh, Y.J. (2005) Eupatilin, a pharmacologically active flavone derived from Artemisia plants, induces apoptosis in human gastric cancer (AGS) cells. *J Environ Pathol Toxicol Oncol*, **24**, 261–269.

40. Wang, Y., Hou, H., Li, M., Yang, Y. and Sun, L. (2016) Anticancer effect of eupatilin on glioma cells through inhibition of the Notch-1 signaling pathway. *Mol Med Rep*, **13**, 1141.

41. Giangaspero, A., Ponti, C., Pollastro, F., Giorgia Favero, D.E.L., Loggia, R. della, Tubaro, A., Appendino, G. and Sosa, S. (2009) Topical Anti-inflammatory Activity of Eupatilin, A Lipophilic Flavonoid from Mountain Wormwood (Artemisia umbelliformis Lam.). *J Agric Food Chem*, **57**, 7726–7730.

42. Choi, E.J., Lee, S., Chae, J.R., Lee, H.S., Jun, C.D. and Kim, S.H. (2011) Eupatilin inhibits lipopolysaccharide-induced expression of inflammatory mediators in macrophages. *Life Sci*, **88**, 1121–1126.

43. Nageen, B., Sarfraz, I., Rasul, A., Hussain, G., Rukhsar, F., Irshad, S., Riaz, A., Selamoglu, Z. and Ali, M. (2018) Eupatilin: a natural pharmacologically active flavone compound with its wide range applications. *https://doi.org/10.1080/10286020.2018.1492565*, **22**, 1–16.

44. SEOL, S.-Y., KIM, M.-H., REW, J.-S. and CHOI, M.-G. (2004) A Phase III Clinical Trial of Stillen(TM) for Erosive Gastritis. *Korean Journal of Gastrointestinal Endoscopy*, 230–236.

45. May-Simera, H.L., Wan, Q., Jha, B.S., Hartford, J., Khristov, V., Dejene, R., Chang, J., Patnaik, S., Lu, Q., Banerjee, P., *et al.* (2018) Primary Cilium-Mediated Retinal Pigment Epithelium Maturation Is Disrupted in Ciliopathy Patient Cells. *Cell Rep*, **22**, 189–205.

46. Ra, R., Yamamoto, E.A., Dewanjee, M., Munasinghe, J., May-Simera, H.L., Dong, L. and Swaroop, A. (2012) CEP290 is required for photoreceptor ciliogenesis and other cilia related functions. *Cilia 2012 1:1*, **1**, 1–1.

47. Potter, V.L., Moye, A.R., Robichaux, M.A. and Wensel, T.G. (2021) Super-resolution microscopy reveals photoreceptor-specific subciliary location and function of ciliopathy-associated protein CEP290. *JCI Insight*, **6**.

48. Mercey, O., Kostic, C., Bertiaux, E., Giroud, A., Sadian, Y., Gaboriau, D.C.A., Morrison, C.G., Chang, N., Arsenijevic, Y., Guichard, P., *et al.* (2022) The connecting cilium inner scaffold provides a structural foundation that protects against retinal degeneration. *PLoS Biol*, **20**, e3001649.

49. Drivas, T.G., Wojno, A.P., Tucker, B.A., Stone, E.M. and Bennett, J. (2015) Basal exon skipping and genetic pleiotropy: A predictive model of disease pathogenesis. *Sci Transl Med*, **7**.

50. Garanto, A., van Beersum, S.E.C., Peters, T.A., Roepman, R., Cremers, F.P.M. and Collin, R.W.J. (2013) Unexpected CEP290 mRNA splicing in a humanized knock-in mouse model for Leber congenital amaurosis. *PLoS One*, **8**.

51. Kruczek, K., Qu, Z., Welby, E., Shimada, H., Hiriyanna, S., English, M.A., Zein, W.M., Brooks, B.P. and Swaroop, A. (2022) In vitro modeling and rescue of ciliopathy associated with IQCB1/NPHP5 mutations using patient-derived cells. *Stem Cell Reports*, **17**, 2172–2186.

52. Kim, J., Krishnaswami, S.R. and Gleeson, J.G. (2008) CEP290 interacts with the centriolar satellite component PCM-1 and is required for Rab8 localization to the primary cilium. *Hum Mol Genet*, **17**, 3796–3805.

53. Prosser, S.L. and Morrison, C.G. (2015) Centrin2 regulates CP110 removal in primary cilium formation. *J Cell Biol*, **208**, 693.

54. Spektor, A., Tsang, W.Y., Khoo, D. and Dynlacht, B.D. (2007) Cep97 and CP110 suppress a cilia assembly program. *Cell*, **130**, 678–690.

55. Tsang, W.Y., Bossard, C., Khanna, H., Peränen, J., Swaroop, A., Malhotra, V. and Dynlacht, B.D. (2008) CP110 Suppresses Primary Cilia Formation through Its Interaction with CEP290, a Protein Deficient in Human Ciliary Disease. *Dev Cell*, **15**, 187–197.

56. Tsang, W.Y., Spektor, A., Luciano, D.J., Indjeian, V.B., Chen, Z., Salisbury, J.L., Sánchez, I. and Dynlacht, B.D. (2006) CP110 cooperates with two calcium-binding proteins to regulate cytokinesis and genome stability. *Mol Biol Cell*, **17**, 3423–3434.

57. Arnon, A., Cook, B., Montell, C., Selinger, Z. and Minke, B. (1997) Calmodulin Regulation of Calcium Stores in Phototransduction of Drosophila. *Science (1979)*, **275**, 1119–1121.

58. Ikura, M., Osawa, M. and Ames, J.B. (2002) The role of calcium-binding proteins in the control of transcription: structure to function. *Bioessays*, **24**, 625–636.

59. Carrión, A.M., Link, W.A., Ledo, F., Mellström, B. and Naranjo, J.R. (1999) DREAM is a Ca2+-regulated transcriptional repressor. *Nature 1999 398:6722*, **398**, 80–84.

60. Naranjo, R., González, P., Lopez-Hurtado, A., Dopazo, X.M., Mellström, B. and Naranjo, J.R. (2018) Inhibition of the neuronal calcium sensor DREAM modulates presenilin-2 endoproteolysis. *Front Mol Neurosci*, **11**, 449.

61. de Oliveira, D.R., Zamberlam, C.R., Rêgo, G.M., Cavalheiro, A., Cerutti, J.M. and Cerutti, S.M. (2016) Effects of a Flavonoid-Rich Fraction on the Acquisition and Extinction of Fear Memory: Pharmacological and Molecular Approaches. *Front Behav Neurosci*, **9**, 345.

62. Cichon, N., Saluk-Bijak, J., Gorniak, L., Przyslo, L. and Bijak, M. (2020) Flavonoids as a Natural Enhancer of Neuroplasticity-An Overview of the Mechanism of Neurorestorative Action. *Antioxidants (Basel)*, **9**, 1–19.

63. Carbonel, A.A.F., Cecyn, M.N., Girão, J.H.R.C., Sasso, G.R. da S., Ponteciano, B. de M., Vellozo, E.P., Simões, R.S., Simões, M. de J., Girão, M.J.B.C. and Oliveira, D.R. de (2019) Flavonoids as Modulators of Synaptic Plasticity: Implications for the Development of Novel Therapeutic Strategies for Healthy Lifestyle. *Flavonoids - A Coloring Model for Cheering up Life*.

64. Kayama, M., Nakazawa, T., Thanos, A., Morizane, Y., Murakami, Y., Theodoropoulou, S., Abe, T., Vavvas, D. and Miller, J.W. (2011) Heat shock protein

70 (HSP70) is critical for the photoreceptor stress response after retinal detachment via modulating anti-apoptotic Akt kinase. *Am J Pathol*, **178**, 1080–1091.

65. Jiang, K., Fairless, E., Kanda, A., Gotoh, N., Cogliati, T., Li, T. and Swaroop, A. (2020) Divergent Effects of HSP70 Overexpression in Photoreceptors During Inherited Retinal Degeneration. *Invest Ophthalmol Vis Sci*, **61**.

66. Deane, C.A.S. and Brown, I.R. (2018) Knockdown of Heat Shock Proteins HSPA6 (Hsp70B') and HSPA1A (Hsp70-1) Sensitizes Differentiated Human Neuronal Cells to Cellular Stress. *Neurochem Res*, **43**, 340–350.

67. Shorbagi, S. and Brown, I.R. (2016) Dynamics of the association of heat shock protein HSPA6 (Hsp70B') and HSPA1A (Hsp70-1) with stress-sensitive cytoplasmic and nuclear structures in differentiated human neuronal cells. *Cell Stress Chaperones*, **21**, 993–1003.

68. Sladen, P.E., Jovanovic, K., Guarascio, R., Ottaviani, D., Salsbury, G., Novoselova, T., Chapple, J.P., Yu-Wai-Man, P. and Cheetham, M.E. (2022) Modelling autosomal dominant optic atrophy associated with OPA1 variants in iPSC-derived retinal ganglion cells. *Hum Mol Genet*, **31**, 3478–3493.

69. Howden, S.E., Thomson, J.A. and Little, M.H. (2018) Simultaneous reprogramming and gene editing of human fibroblasts. *Nature Protocols 2018 13:5*, **13**, 875–898.

70. Okita, K., Matsumura, Y., Sato, Y., Okada, A., Morizane, A., Okamoto, S., Hong, H., Nakagawa, M., Tanabe, K., Tezuka, K.I., *et al.* (2011) A more efficient method to generate integration-free human iPS cells. *Nature Methods 2011 8:5*, **8**, 409–412.

71. Schwarz, N., Carr, A.J., Lane, A., Moeller, F., Chen, L.L., Aguilà, M., Nommiste, B., Muthiah, M.N., Kanuga, N., Wolfrum, U., *et al.* (2015) Translational read-through of the RP2 Arg120stop mutation in patient iPSC-derived retinal pigment epithelium cells. *Hum Mol Genet*, **24**, 972–986.

72. Love, M.I., Huber, W. and Anders, S. (2014) Moderated estimation of fold change and dispersion for RNA-seq data with DESeq2. *Genome Biol*, **15**, 1–21.

73. Zhu, A., Ibrahim, J.G. and Love, M.I. (2019) Heavy-tailed prior distributions for sequence count data: removing the noise and preserving large differences. *Bioinformatics*, **35**, 2084–2092.

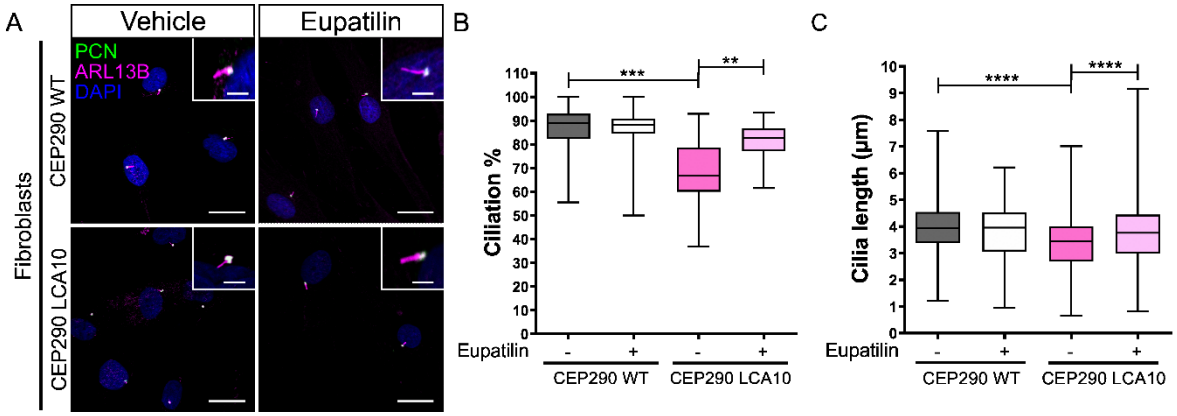

Figure 1. Eupatilin increases cilia incidence and length in CEP290 LCA10 patient fibroblasts. A, Representative images of control (CEP290 WT) and CEP290 LCA10 fibroblasts treated with eupatilin (20 µM) or vehicle, stained for pericentrin (PCN, green, basal body) and ARL13b (magenta, axoneme). Scale bar: 20 µm. Inset shows cilia at higher magnification. Scale bar 5 µm. **B-C**, Cilia incidence and length were scored using the elaboration of an ARL13B positive axoneme from a PCN positive basal body. Number of cilia counted in B: WT vehicle (-) n=89, Eupatilin (+) n=147; CEP290 LCA10 vehicle (-) n=99, Eupatilin (+) n=87 (B). Number of cilia counted in C: WT vehicle (-) n=271, Eupatilin (+) n=231; CEP290 LCA10 vehicle (-) n=214, Eupatilin (+) n=345. Mean ± standard deviation (SD), ** P<0.01, *** P<0.005, **** p<0.0001 one-way ANOVA test.

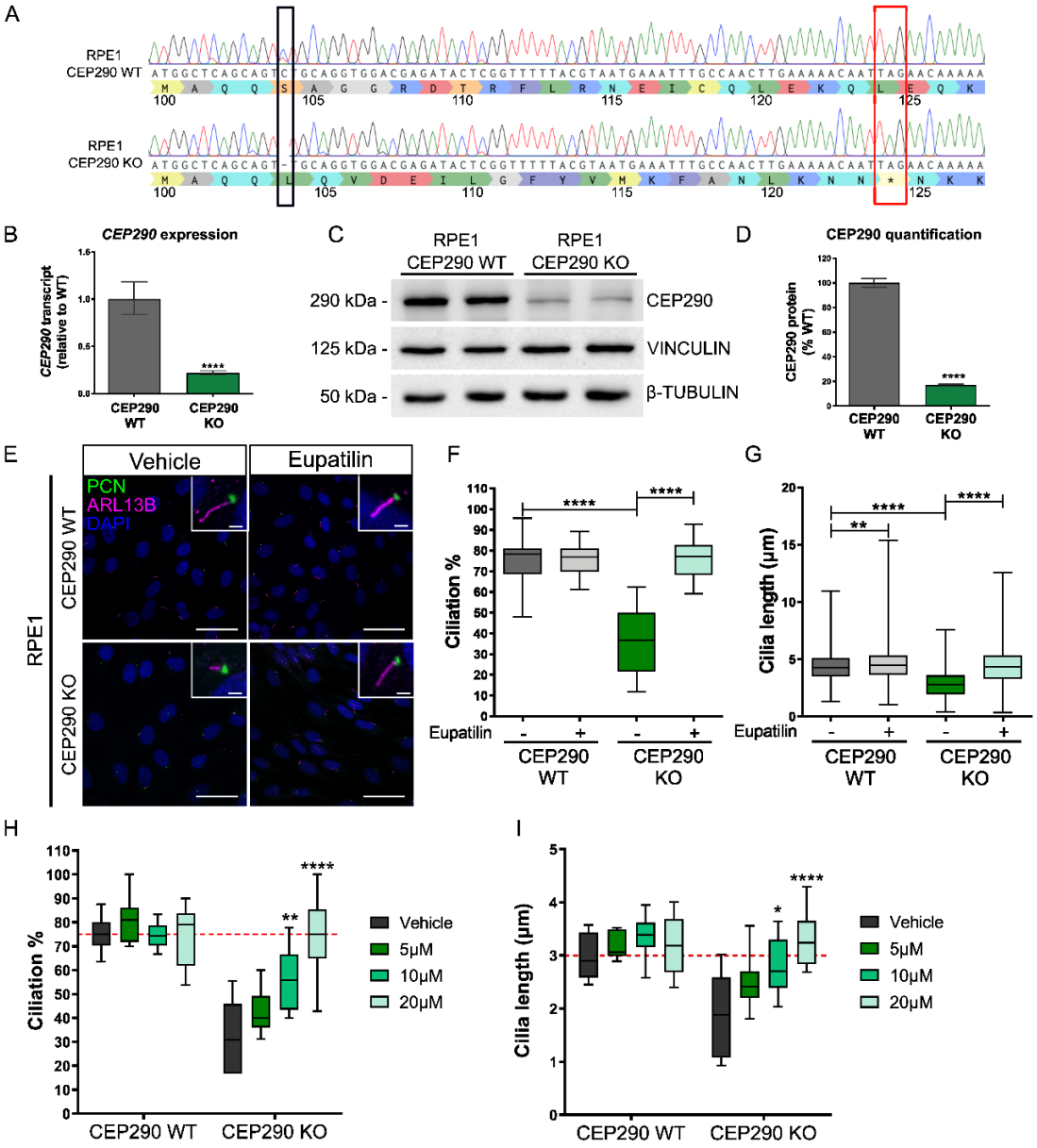

Figure 2. Eupatilin improves cilia incidence and length in CEP290 KO RPE1 cells. **A**, Sanger sequence showing CRISPR/Cas9-induced deletion of 1 bp in *CEP290* (black box) and predicted effect on amino acid sequence. Stop codon is highlighted in exon 6 (red box). **B,** qPCR analyses of *CEP290* transcripts shows reduced levels in CEP290 KO RPE1 cells. Primers were designed between exon 13 and 14, n=4. **C,** Western blot of CEP290 protein shows reduced level in CEP290 KO cells, β-tubulin and vinculin were used as reference proteins. **D**, Quantification of western blot, showing reduced CEP290 expression. n=3 independent western blots. **E**, Representative images of CEP290 WT (control) and CEP290 KO RPE1 cells treated with vehicle or eupatilin (20 μM) with cilia stained for PCN (green) and ARL13b (magenta). Scale bar: 40 μm. Inset shows cilium at higher magnification. Scale bar: 2 μm. Graphical representation of cilia incidence (**F**), and cilia length (**G**), in WT and CEP290 KO RPE1 cells treated with 20 μM eupatilin. **F-G,** 24-28 independent fields of view, from 3 separate experiment repeats were scored, and 207-630 cilia were measured. **H-I**, The effect of eupatilin treatment for 24 hours at the indicated doses on cilia incidence and length was measured. **H,** 8 independent images, from 2 separate experiment repeats were scored, and

19-92 cilia were measured (**I**). Median ± min and max, ** p<0.01, *** p<0.005, **** p<0.0001 ordinary one-way ANOVA with Tukey's post-hoc test.

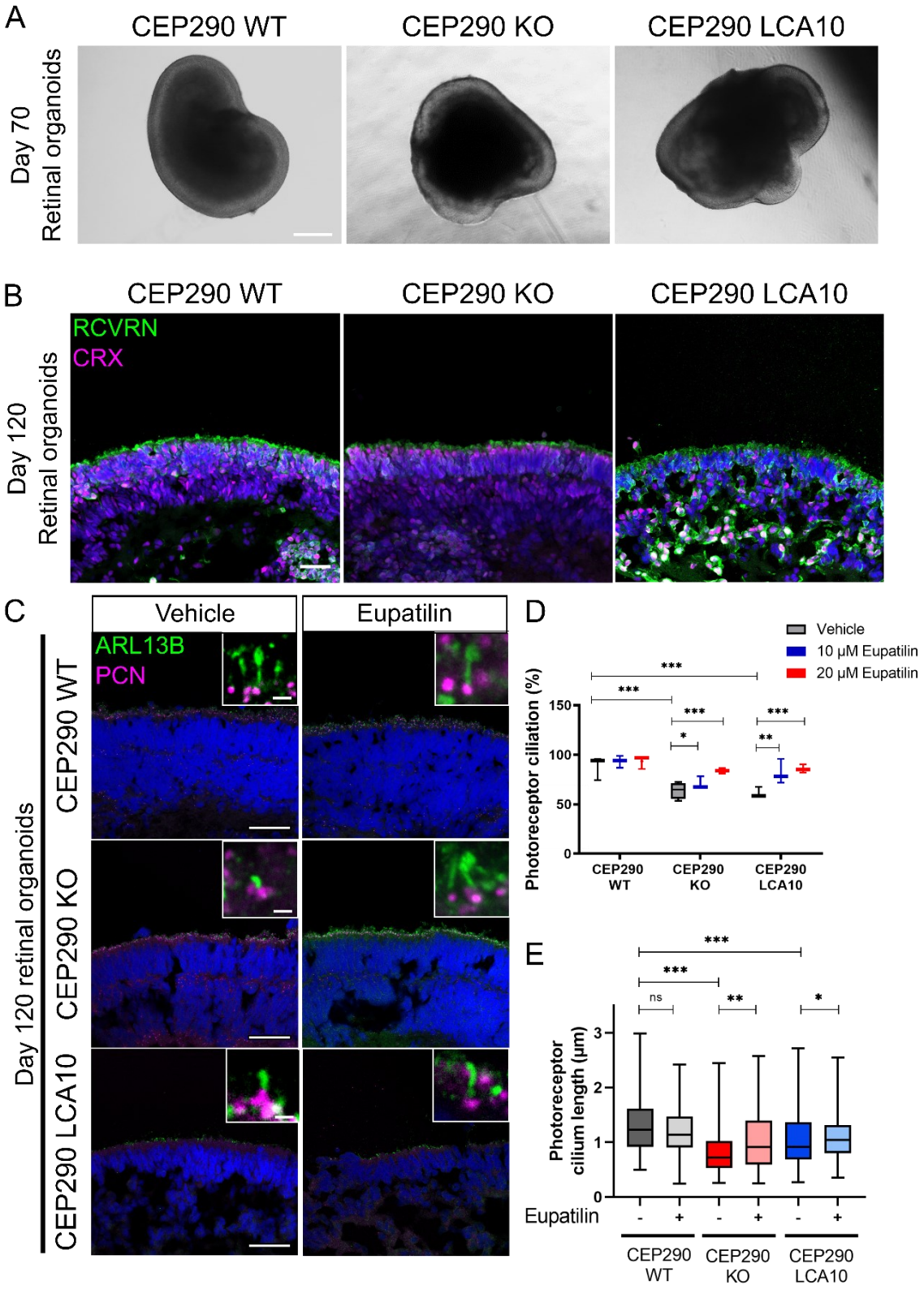

Figure 3. Eupatilin treatment restores ciliation and cilia length in iPSC-derived CEP290 KO and CEP290 LCA10 retinal organoids. **A**, Bright field images of CEP290 retinal organoids at differentiation day 70. Scale bar: 500 μm. **B**, RCVRN (green) and CRX

(magenta) staining of day 120 retinal organoids. Scale bar: 40 µm **C**, Eupatilin treatment of retinal organoids from days 90 to 120. Cilia were stained with ARL13B (green) and PCN (magenta). Scale bar: 40 µm. Insets show a higher magnification of the photoreceptor cilia. Scale bar: 1 µm **D,** Quantification of photoreceptor ciliation and photoreceptor cilium length (**E**) in CEP290 retinal organoids at day 120 after eupatilin treatments. CEP290 WT Vehicle n=4 ROs (141 cilia), CEP290 WT EUP n=4 ROs (135 cilia), CEP290 KO Vehicle n=3 (148 cilia), CEP290 KO EUP n=2 (88 cilia), CEP290 LCA10 Vehicle n=4 (114 cilia), CEP290 LCA10 EUP n=4 (176 cilia). * p<0.05 ** p<0.01, *** P<0.001, ordinary one-way ANOVA with Tukey's post-hoc test.

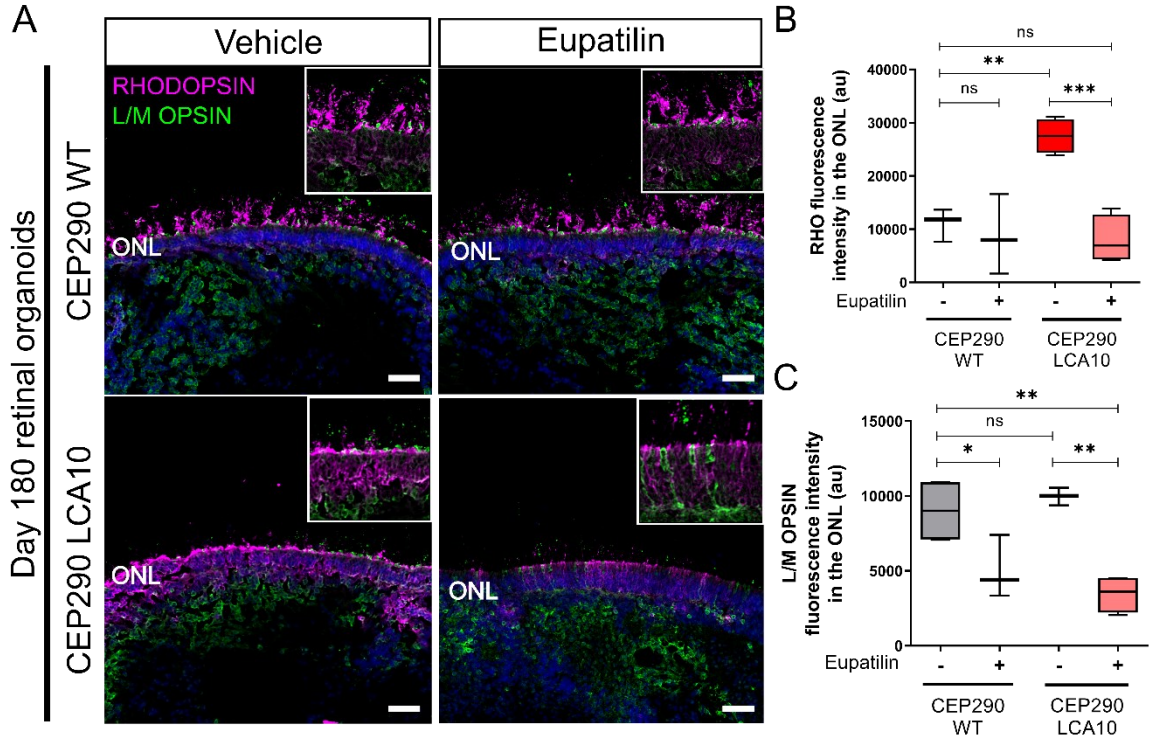

Figure 4. Opsin accumulates in the outer nuclear layer of CEP290 LCA10 retinal organoids and is rescued by eupatilin. **A**, Representative images of CEP290 WT (control) and CEP290 LCA10 retinal organoids at D180 treated with eupatilin (20 µM) or vehicle for 30 days (from D150), stained for rhodopsin (magenta) and L/M opsin (green). Photoreceptor nuclei were stained with DAPI (blue). Scale bar: 10 µm. **B**, Quantification of RHO and L/M opsin (**C**) immunofluorescence intensity in the photoreceptor outer nuclear layer (ONL). Each data point represents the mean of 3 measurements from one organoid, bar represents mean ± SD. * p<0.05 ** p<0.01, *** P<0.001.

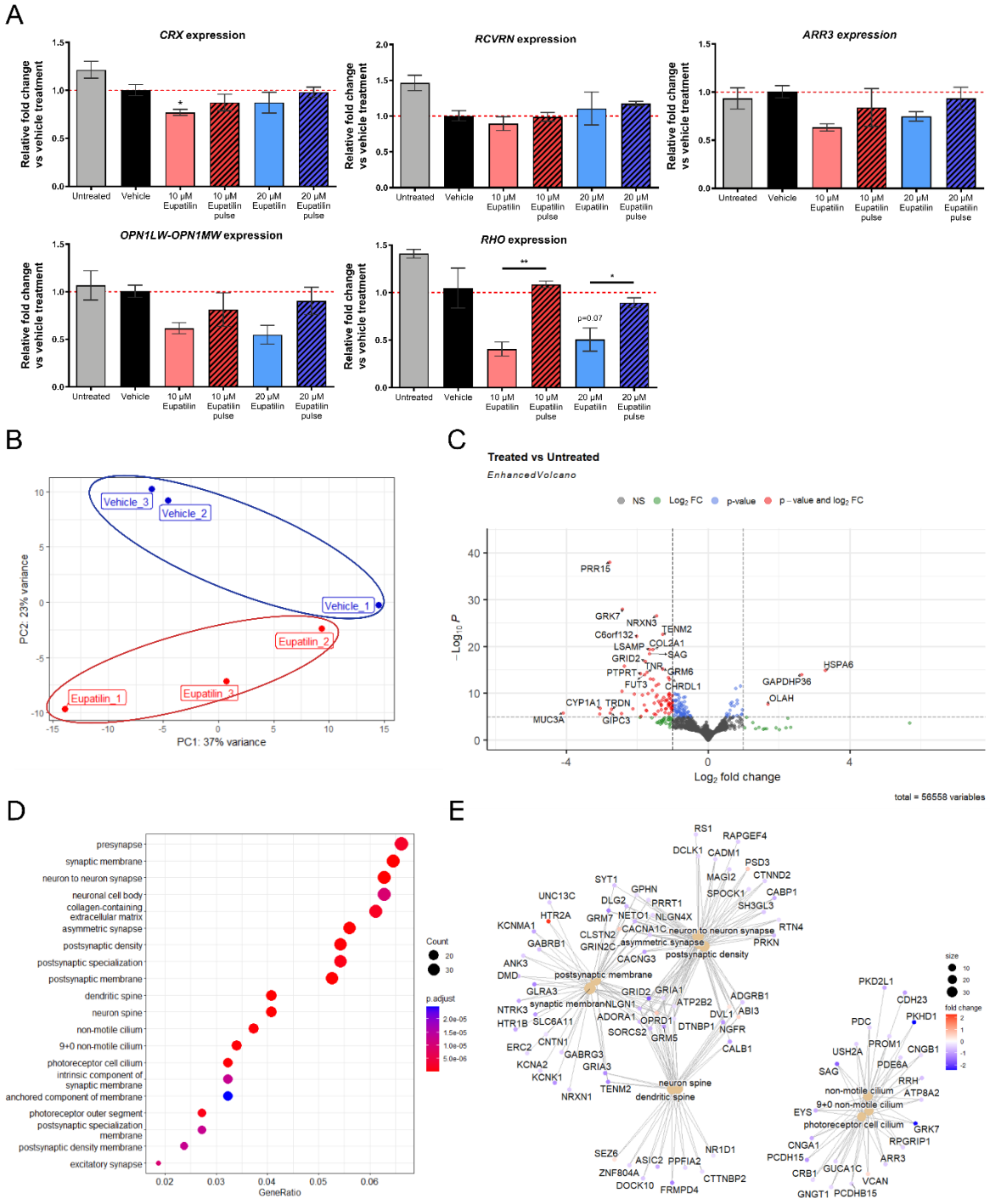

Figure 5. Transcriptome analysis of eupatilin treated control retinal organoids. A, The effect of eupatilin on of *CRX*, *ARR3*, *RCVRN*, *RHO*, *OPN1LW-OPN1MW* gene expression by qPCR. Day 250 control retinal organoids were treated with vehicle (DMSO) or eupatilin at the indicated concentrations for 14 days and harvested or allowed to recover for 14 days with no treatment ('pulse'), untreated organoids are shown at D250 for comparison. qPCR analyses. Means ± SD n=3 independent retinal organoids, * p<0.05 ** p<0.01, one-way ANOVA with Tukey's post-hoc test. Effect of eupatilin on the transcriptome by. Bulk RNA sequencing was performed on day 240 organoids after 1 month eupatilin treatment. **B**, PCA analyses showing separation between the eupatilin treated organoids and the vehicle treated organoids by PC2 variance. **C**, Volcano plot showing the most differentially expressed genes. **D**, Dotplot showing

the top 20 gene ontology (GO) cellular components by over-representation analysis. **E**, Netplot showing the relationship between the top 10 most enriched gene ontology terms and their genes.

Supplemental material

Eupatilin improves cilia defects in human CEP290 ciliopathy models

Corral-Serrano, Sladen, Ottaviani et al.

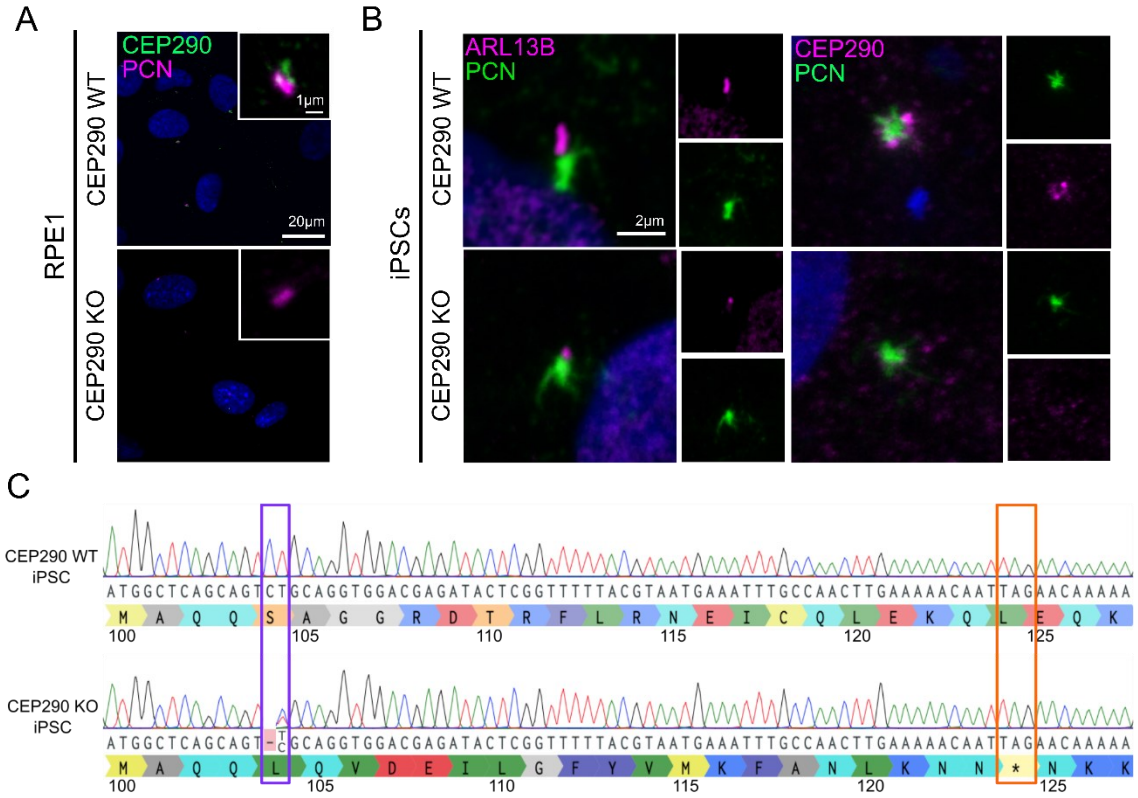

Supplementary Figure 1. CEP290 localization in CEP290 RPE1 and iPSCs KO cells. A, Immunofluorescence staining of CEP290 WT and CEP290 KO RPE1 cells showing cilia staining of pericentrin (PCN, magenta) and CEP290 (green). CEP290 staining shows expression in the CEP290 WT line while the CEP290 protein is absent in the cilia of CEP290 KO RPE1. Insets show a magnification of both channels. Scale = 1 µm. **B**, Immunofluorescence staining of CEP290 WT and CEP290 KO iPSC showing cilia staining of: upper panels, ARL13B (magenta) and pericentrin (PCN, green); lower panels CEP290 (magenta) and pericentrin (PCN, green). CEP290 staining shows expression in the CEP290 WT while the CEP290 protein is absent in the cilia of CEP290 KO iPSC. Insets show the split of both channels. Scale = 2 µm. **C,** Production of CEP290 KO iPSC. Sanger sequence trace showing compound heterozygous 1 bp deletion (purple box) in CEP290 KO iPSC leading to frame shift and premature stop codon (orange box).

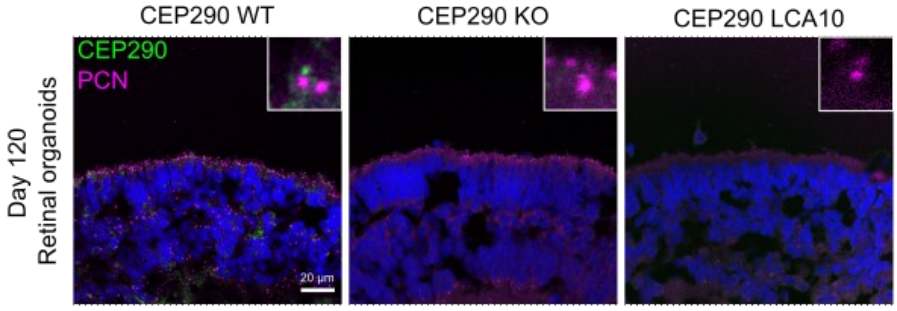

Supplementary Figure 2. CEP290 protein localization in retinal organoids. CEP290 antibody staining in day 120 retinal organoids shows absence of CEP290 in both CEP290 KO and CEP290 LCA10 organoids. Organoids were stained with a CEP290 antibody (green) and a PCN antibody (magenta). Scale bar = 20 µm.

Supplementary Table 1. List of primers used in this study.

qPCR

Gene	Primer	
	Forward	**Reverse**
ACTIN	CCAACCGCGAGAAGATGA	CCAGAGGCGTACAGGGATAG
ARR3	CAGCTCAGCCCCTACAACTC	ACTGCAAAGCTCTGGGAGAA
CRX	TTTGCCAAGACCCAGTACC	GTTCTTGAACCAAACCTGAACC
GAPDH	CCCCACCACACTGAATCTCC	GGTACTTTATTGATGGTACATGACAAG
OPN1LW/ OPN1MW	CATCCGAGCGGTGGCAAAGC	CAGCAGAATGCCAGGACCATC
RECOVERIN	AGCTCCTTCCAGACGATGAA	CAAACTGGATCAGTCGCAGA
RHO	GGTGGTGTGTAAGCCCATGA	CCTCGGGGATGTACCTGGAC

CEP290 sequencing

Gene	Primer	
	Forward	**Reverse**
CEP290 exon 6 pair 1	GGCCCAGTGGTTACAACAG	GGTGATGACAAAATGAACAGTGA
CEP290 exon 6 pair 2	CTTTGCATCTCTGGGTGGCTC	ACCAATCTTCCAGACAAAAGCA